Aerodynamic effect of non-uniform wind profiles for long-span bridges

Tor M. Lystad[1, 2,*], Aksel Fenerci[2] and Ole Øiseth[2]

[1] Bridge Department, Norconsult
1338, Sandvika (Norway)
tor.martin.lystad@norconsult.com

[2] Department of Structural Engineering, Norwegian University of Science and Technology,
7034, Trondheim, (Norway)

Abstract Long-span bridges are often designed based on the assumption of wind field homogeneity. At the Hardanger Bridge, the wind field along the bridge span is monitored though 8 3d ultrasonic anemometers. Simultaneously recorded profiles for mean wind velocity and turbulence intensity along the span are used to investigate the effect of non-uniform wind profiles on the aerodynamic behaviour of the Hardanger Bridge. Extreme non-uniformity is considered using Monte Carlo simulations to generate extreme, but realistic wind profiles based on the variability of the measured wind field. When the buffeting response of the Hardanger Bridge is considered, significant effects on the behaviour is found.

Keywords: Long-span bridge · Non-uniform wind field · Field measurements · Complex terrain

1 Introduction

Long-span bridges located in complex terrain can be subjected to large wind field variations along the bridge span, as shown in Lystad et al. (2018). Long-span bridges are often designed under the assumption of wind field homogeneity, however this assumption may not be valid for bridges located in complex terrain such as the mountainous landscape along the west coast of Norway.

Since 2013 the Norwegian University of Science and Technology has been monitoring the wind field along the Hardanger Bridge girder through 8 triaxial ultrasonic anemometers. The Hardanger Bridge is a suspension bridge with a main span of 1 310 m, located in complex terrain. The measured wind field display large non-uniformity along the bridge span.

The effect of idealized non-uniform mean wind velocity profiles on the buffeting response and the aerodynamic stability of long-span bridges has been studied by (Arena et al. 2014; Zhang 2007), showing possible significant effects on the aerodynamic behavior. A non-uniform mean wind velocity profile measured from terrain model wind tunnel tests of the Stonecutters Bridge surroundings was also investigated

in (Hu et al. 2017), without any significant impacts to the bridge behavior. However, to the authors knowledge, investigations of the effect of extreme, but realistic non-uniform wind profiles based on full-scale measurements has not been treated in the literature.

In this paper, non-uniform profiles of mean wind velocity and turbulence intensity measured in full-scale at the Hardanger Bridge site are investigated. A measure of the variability of the recorded non-uniformity is obtained by fitting the measured wind profiles to chosen shape functions using linear regression. Profiles of mean wind velocity and corresponding turbulence intensity are generated through Monte Carlo simulations from the joint probability distribution of the fitted shape function coefficients. Finally, the effect of some simulated extreme non-uniform wind profiles on the buffeting response of the Hardanger Bridge are shown.

2 Full-scale measurement program

The Hardanger Bridge is a suspension bridge with a main span of 1 310 m, located along the west coast of Norway. The bridge is crossing the Hardanger fjord surrounded by tall and steep mountains, forming a very complex topography.

Since the opening of the bridge in 2013, a monitoring system has been recording the wind field along the bridge span as well as in the southern tower top. Also, acceleration response of the girder and towers has been recorded. An overview of the wind measurement system is given in Fig. 1 and the system is described in more detail in (Fenerci et al. 2017).

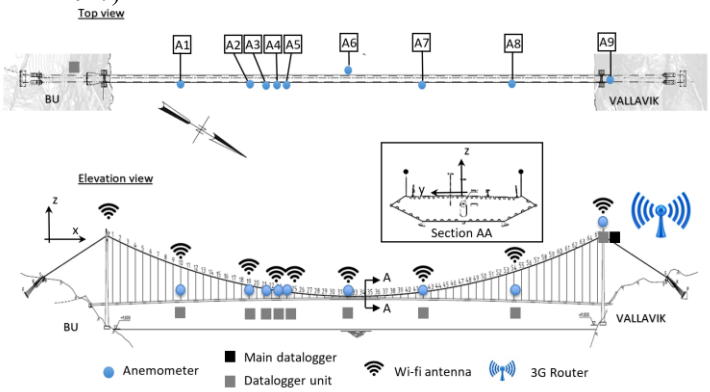

Fig. 1 Overview of the full-scale wind measurement system at the Hardanger Bridge

The Hardanger fjord is creating strong orographic channelling effects on the wind field subjected to the bridge structure, generating two very distinct incoming wind directions from the east and west. This behaviour can be observed in Fig. 2, where the midspan wind rose for strong winds with mean wind velocities above 15 m/s is shown. The wind rose shown in Fig. 2 is plotted on top of a map showing the surrounding

topography, and it should be noted that the surrounding mountains reach up to above 1000 m. For a more thorough description of the surrounding topography, the reader is referred to (Fenerci et al. 2017; Fenerci and Øiseth 2017; Lystad et al. 2018).

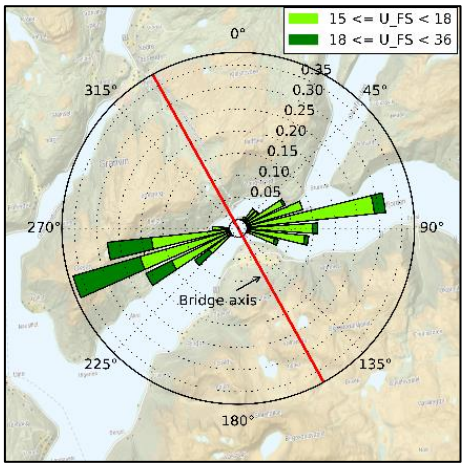

Fig. 2 Mean wind velocity rose for strong winds above 15 m/s, measured in the midspan. The wind rose is divided into two main wind directions, east and west, with each side adding up to 100% (base map with courtesy of Kartverket©)

3 Non-uniform wind profiles

3.1 Measurements

Along-span wind profiles for mean wind velocity and along-wind turbulence intensity for strong winds recorded at the Hardanger Bridge are shown in Fig. 3. Only measurements with a midspan 10-min time-averaged mean wind velocity above 15 m/s are considered, and extreme non-uniform measured profiles are highlighted.

By observing the general shape of the measured profiles, it is seen that the profiles may be described quite well by the combination of a linear variation and a cosine function. The following wind profile model is proposed:

$$U(x) = U_0 + a_1 x - a_2[1-\cos(\frac{\pi}{L}x)] = U_0\{1+\hat{a}_1 x - \hat{a}_2[1-\cos(\frac{\pi}{L}x)]\} \quad (1)$$

$$I(x) = I_0 + b_1 x - b_2[1-\cos(\frac{\pi}{L}x)] = I_0\{1+\hat{b}_1 x - \hat{b}_2[1-\cos(\frac{\pi}{L}x)]\} \quad (2)$$

where the a_1, and b_1 coefficients describe the linear variation and the a_2, and b_2 coefficients scale the cosine shape function. Another model for the non-uniformity of the

mean wind velocity was shown in Zhang (2007), but this model is deemed less suitable for the methodology described in the present study.

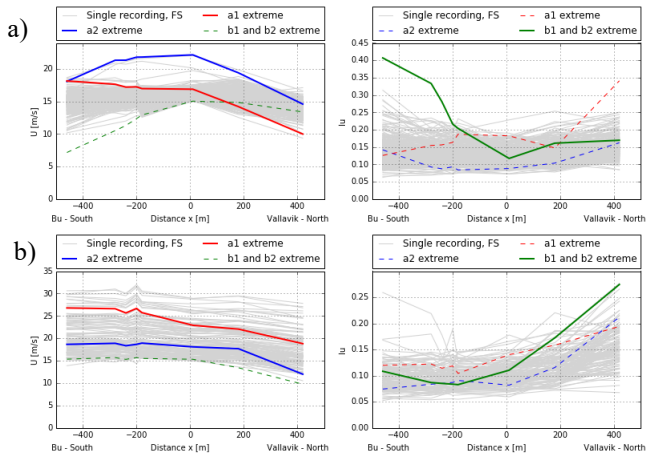

Fig. 3 Measured wind profiles and highlighted extreme non-uniformity a) The wind recordings of easterly winds and b) recordings of westerly winds.

For comparison of the non-uniformity effect it is interesting to consider wind profiles with the same along span mean value. To achieve this the midspan value of the wind profile, U_0 and I_0, and thus the normalized non-uniformity coefficients $\hat{a}_i$ and $\hat{b}_i$ are scaled based on Eq. (3) and (4), demanding the same along span mean values, U_{eq} and I_{eq} for all profiles.

$$U_{eq} = \frac{1}{L}\int_{-L/2}^{L/2} U(x)dx = U_0[1-\hat{a}_2 + \frac{2}{\pi}\hat{a}_2] \tag{3}$$

$$I_{eq} = \frac{1}{L}\int_{-L/2}^{L/2} I(x)dx = I_0[1-\hat{b}_2 + \frac{2}{\pi}\hat{b}_2] \tag{4}$$

Using linear regression, the non-uniform wind profile models described in Eq. (1)-(4) are fitted to all measured wind profiles shown in Fig. 3. By doing so, the distribution of the normalized fitted coefficients, $\hat{a}_i$ and $\hat{b}_i$, can be obtained and a probability distribution can be adopted. The mean wind velocity profiles and the corresponding along-wind turbulence intensity profiles are used, so the joint probability density function (PDF) of all the normalized coefficients, $\hat{a}_1$, $\hat{a}_2$, $\hat{b}_1$ and $\hat{b}_2$ can be fitted. A normal distribution is assumed in the present study for the simplicity of describing a joint PDF.

Table 1 Key statistics for the fitted normalized non-uniformity coefficients

	Easterly winds		Westerly winds	
Coeff	Mean	Std	Mean	Std
$\hat{a}_1$	-6.84E-05	1.37E-04	-1.92E-04	1.26E-04
$\hat{a}_2$	9.31E-02	5.64E-02	5.02E-02	4.26E-02
$\hat{b}_1$	1.33E-04	4.28E-04	7.19E-04	4.89E-04
$\hat{b}_2$	-1.70E-01	2.27E-01	-2.67E-01	2.37E-01

Table 2 Correlation coefficients for the normalized non-uniformity coefficients for easterly winds

Coeff	$\hat{a}_1$	$\hat{a}_2$	$\hat{b}_1$	$\hat{b}_2$
$\hat{a}_1$	1.000	0.136	-0.784	-0.151
$\hat{a}_2$	0.136	1.000	-0.208	-0.704
$\hat{b}_1$	-0.784	-0.208	1.000	0.111
$\hat{b}_2$	-0.151	-0.704	0.111	1.000

Table 3 Correlation coefficients for the normalized non-uniformity coefficients for westerly winds

Coeff	$\hat{a}_1$	$\hat{a}_2$	$\hat{b}_1$	$\hat{b}_2$
$\hat{a}_1$	1.000	-0.390	-0.504	0.215
$\hat{a}_2$	-0.390	1.000	0.465	-0.502
$\hat{b}_1$	-0.504	0.465	1.000	-0.657
$\hat{b}_2$	0.215	-0.502	-0.657	1.000

It can be observed from Table 1 that the mean value of the linear variation described by $\hat{a}_1$ and $\hat{b}_1$ is larger for the westerly winds than the easterly winds, confirming the qualitative observation made from Fig. 3. However, considering the cosine shape function coefficients $\hat{a}_2$ and $\hat{b}_2$ the easterly winds are displaying the largest mean value for the normalized non-uniformity coefficient for the mean wind velocity profiles, but the westerly winds are showing generally larger non-uniformity in the turbulence intensity profile.

A high correlation between $\hat{a}_i$ and $\hat{b}_i$ in mean wind velocity and turbulence intensity can be expected, as the turbulence intensity is, by definition, inversely proportional to the mean wind velocity. By studying Table 2 this expected effect is observed as the correlation between $\hat{a}_1$ and $\hat{b}_1$, and $\hat{a}_2$ and $\hat{b}_2$ is in the range of 70-80 %. However, by studying the westerly winds in Table 3 a larger randomness is observed in the correlation coefficients.

3.2 Simulations

Based on the fitted joint PDF of the normalized non-uniformity coefficients, Monte Carlo simulations can be applied to generate a large number of non-uniform wind profiles. The simulations are based on a chosen equivalent mean wind velocity of 40 m/s and an equivalent along-wind turbulence intensity of 15%. The fitted coefficients are

generally based on lower measured wind speeds than the chosen equivalent mean wind velocity, but utilizing the normalized format of the non-uniformity coefficients it is interesting to investigate the effects of the observed non-uniformity at design wind speed levels. Extreme, but realistic, simulated profiles may be picked based on a chosen criterion. In this study the simulations are sorted in ascending order based on the absolute value of the normalized non-uniformity profiles, $\hat{a}_i$ and $\hat{b}_i$. To obtain an extreme non-uniform situation from the simulated profiles the nearest-rank method may be applied to the sorted lists of simulations for each normalized non-uniformity coefficient. Let, *N*, be the number of simulations and, *n*, be the simulation number in the sorted list, the simulated profile with a chosen percentile may be calculated as

$$n = \left\lceil \frac{P}{100} N \right\rceil \tag{5}$$

In Fig. 4, *N=1000* simulated profiles for each main wind direction, westerly and easterly winds, are shown.

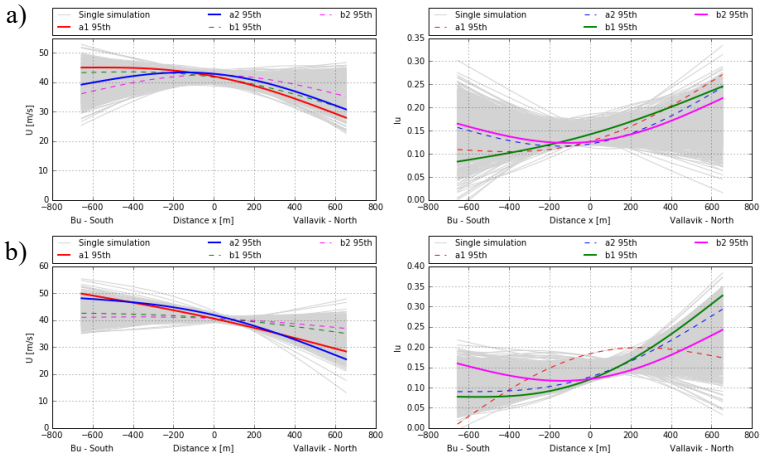

Fig. 4 Monte Carlo simulated wind profiles for a) easterly winds and b) westerly winds. Extreme simulations are highlighted along with the simulation of the corresponding variable (dotted).

The picked extreme mean wind velocity and along-wind turbulence intensity profiles according to the criterion described above, are highlighted and shown in Table 4. Significant non-uniformity in the extreme simulated wind profiles both for mean wind velocity and along-wind turbulence intensity can be observed.

Table 4 Model coefficients for the highlighted extreme non-uniformity profiles

Wind dir	Extreme type	U_0	$\hat{a}_1$	$\hat{a}_2$	I_0	$\hat{b}_1$	$\hat{b}_2$
East	$\hat{a}_{1,95th}$	42.02	-3.10E-04	1.32E-01	0.13	9.72E-04	-4.94E-01
	$\hat{\boldsymbol{a}}_{\boldsymbol{2,95th}}$	**42.87**	**-1.50E-04**	**1.84E-01**	**0.12**	**5.48E-04**	**-6.51E-01**
	$\hat{b}_{1,95th}$	41.69	-2.28E-04	1.12E-01	0.14	8.75E-04	-1.58E-01
	$\hat{b}_{2,95th}$	42.49	-1.64E-05	1.61E-01	0.13	3.35E-04	-5.31E-01
West	$\hat{a}_{1,95th}$	40.53	-4.04E-04	3.61E-02	0.18	6.82E-04	5.01E-01
	$\hat{a}_{2,95th}$	41.85	-4.12E-04	1.22E-01	0.13	1.23E-03	-5.18E-01
	$\hat{\boldsymbol{b}}_{\boldsymbol{1,95th}}$	**40.69**	**-1.41E-04**	**4.69E-02**	**0.12**	**1.59E-03**	**-6.83E-01**
	$\hat{b}_{2,95th}$	40.60	-7.74E-05	4.04E-02	0.12	5.25E-04	-6.61E-01

4 Case study: The Hardanger Bridge

4.1 Theoretical background

The effect of the simulated extreme non-uniform wind profiles on the dynamic response of The Hardanger Bridge is investigated. The Hardanger Bridge is a symmetrical suspension bridge with a main span of 1 310 m and no side spans.

The response calculations are performed in the frequency domain using the multimode theory described in (Chen et al. 2001; Jain et al. 1996a; b). The equation of motion of the dynamic system can be described in the frequency domain as

$$\begin{aligned}&\mathbf{M}_S\mathbf{G}_{\ddot{\eta}}(\omega)+[\mathbf{C}_S-\mathbf{C}_{ae}(U,\omega)]\mathbf{G}_{\dot{\eta}}(\omega)\\&+[\mathbf{K}_S-\mathbf{K}_{ae}(U,\omega)]\mathbf{G}_{\eta}(\omega)=\mathbf{G}_{\mathbf{Q}_{load}}(U,\omega)\end{aligned} \tag{6}$$

where ω is the angular frequency, $\mathbf{M}_S$, $\mathbf{C}_S$ and $\mathbf{K}_S$, are the structural mass-, damping- and stiffness matrices, respectively, in modal coordinates. $\mathbf{C}_{ae}$ and $\mathbf{K}_{ae}$, are the aeroelastic damping and stiffness matrices respectively, representing the motion induced forces. $\mathbf{G}_{\eta}$, $\mathbf{G}_{\dot{\eta}}$, $\mathbf{G}_{\ddot{\eta}}$ and $\mathbf{G}_{\mathbf{Q}_{load}}$ are the Fourier transforms of the displacement-, velocity-, acceleration response and the load process, respectively. In practice, the structural part of the equation has been calculated based on the finite element method, with ABAQUS (Dassault Systèmes, Waltham n.d.), and the aeroelastic motion induced forces are described based on wind tunnel experiments (Siedziako et al. 2017).

The wind field is described as a stationary stochastic process through the cross-spectral density matrix

$$\mathbf{S}_V(\Delta x,U,\omega)=\begin{bmatrix}S_{uu}(\Delta x,U,\omega) & S_{uw}(\Delta x,U,\omega)\\ S_{uw}(\Delta x,U,\omega) & S_{ww}(\Delta x,U,\omega)\end{bmatrix} \tag{7}$$

where S_{nm} are the cross spectral densities for the n and m components of the turbulence between two points separated in space by the distance Δx. In the current study, the off-diagonal terms of the cross-spectral density matrix are assumed to be negligible. The cross-spectral density for a single turbulence component can be described through the auto-spectral density function and the normalized co-spectra:

$$S_{nn}(\Delta x, U, \omega) = S_n(U, I_n, \omega) C(\Delta x, U, \omega) \tag{8}$$

$$C(\Delta x, \omega) = \exp(-K \frac{\omega \Delta x}{2\pi U}) \tag{9}$$

where S_n is the auto-spectral density function, C is the normalized co-spectra, and K is the decay coefficient. Having established the cross-spectral density matrix for the wind field process the spectral matrix of the buffeting force on the structure in modal coordinates can be defined as

$$\mathbf{S}_{Q_{load}} = \iint_L \Phi^T(x_1) \mathbf{B}_q(U, \omega) \mathbf{S}_V(\Delta x, \omega) \mathbf{B}_q^T(U, \omega) \Phi(x_2) dx_1 dx_2 \tag{10}$$

where $\Phi(x_i)$ is the mode shape matrix and $\mathbf{B}_q$ is the load transfer matrix for the buffeting load on the structure. The load spectral density matrix is calculated by considering two points at a time, x_1 and x_2. Having a non-uniform wind field, the mean wind velocity and turbulence intensity will differ at the two points considered, so an adjustment to the original buffeting theory first described by (Davenport 1962; Scanlan and Tomko 1971) has to be made. In the present study, a simple adjustment is done by defining the cross-spectral density for the considered turbulence component as the product of the square root of the auto-spectral density in each point and a normalized co-spectra based on the average of the mean wind velocity from the two points considered. Hence, the following adjustment can be made to Eq. (8):

$$\begin{aligned} &S_{nn}[\Delta x, U(x_1), U(x_2), \omega] = \\ &\sqrt{S_n[U(x_1), I_n(x_1), \omega]} \sqrt{S_n[U(x_2), I_n(x_2), \omega]} C(\Delta x, U_{avrg}, \omega) \end{aligned} \tag{11}$$

where $U_{avrg}=[U(x_1) + U(x_2)]/2$.

The buffeting load transfer matrix is also a function of the mean wind velocity, and to account for the non-uniformity the buffeting matrix corresponding to each of the points considered in Eq. (10), it is adjusted using the actual mean wind velocity in that point. Thus, the cross-spectral density matrix for the buffeting force on the structure can be redefined as

$$\begin{aligned} \mathbf{S}_{Q_{load}} = \iint_L &\{\Phi^T(x_1) \mathbf{B}_q[U(x_1), \omega] \mathbf{S}_V[\Delta x, U(x_1), U(x_2), \omega] \\ &\mathbf{B}_q^T[U(x_2), \omega] \Phi(x_2)\} dx_1 dx_2 \end{aligned} \tag{12}$$

The motion induced forces are integrated using the full non-uniform mean wind velocity profile as follows:

$$\tilde{\mathbf{K}}_{ae}(U(x),\omega) = \int_L \Phi^T \mathbf{K}_{ae}(U(x),\omega)\Phi dx \tag{13}$$

$$\tilde{\mathbf{C}}_{ae}(U(x),\omega) = \int_L \Phi^T \mathbf{C}_{ae}(U(x),\omega)\Phi dx \tag{14}$$

where $\mathbf{K}_{ae}$, and $\mathbf{C}_{ae}$ are described by the dimensionless aerodynamic derivatives.

4.2 Results

Using the methodology described above, the buffeting short-term extreme value for the horizontal, vertical and torsional displacement responses as well as the bending- and torsional cross-sectional moments has been calculated for the Hardanger Bridge girder. The tested extreme non-uniformity profiles are the cosine shaped extreme for the mean wind velocity from the easterly direction and the linearly varying extreme along-wind turbulence intensity profile for the westerly winds, highlighted in Table 4 and shown again in Fig. 5. Only the along-wind turbulence intensity is based on the full-scale measurements in this study, and the vertical component is assumed to be 50% of the along-wind component, adopting the same along span profile shape.

Significant effects on the response can be observed in Fig. 6, for all response quantities considered. For the *a2east* profile all buffeting response quantities are lower than for the uniform situation. The reason for this is the opposite trends of the mean wind velocity and the turbulence intensity, cancelling each other out when considering buffeting action. A combination like this is natural, since the turbulence intensity is inverse proportional to the mean wind velocity. This observed effect highlights the limitations of the simple sorting criterion used in the present study where only extreme non-uniformity for each variable, either mean wind velocity or turbulence intensity, is sorted, and the corresponding profile has no influence on the sorting criterion. Adopting such an approach would not be suitable to identify the combined extreme non-uniformity situation for the considered bridge response, but merely to identify extreme profiles for the purpose of illustration. Also, different sorting criterions would be appropriate for the consideration of different response processes. For instance, an unfavorable combination of mean wind velocity and turbulence intensity would be critical for the buffeting response, but considering flutter instability the mean wind velocity is the driving process and an extreme mean wind velocity profile should be chosen with less emphasis on the combination with turbulence intensity. Possible sorting criterions for the simulated non-uniformity profiles are not investigated in the present study and could be subject for further work on this topic.

Although a cancelling out effect is observed for the considered *a2east* profiles, the *b1west* simulation show unfavorable conditions for the buffeting response of the Hardanger Bridge. The very high turbulence intensity towards the north end of the bridge is generating large responses for all sectional moments shown in Fig. 6. Especially the weak axis moment, *SM1*, shows an underestimation of about 25% using the uniformity assumption compared with the simulated extreme non-uniformity profile.

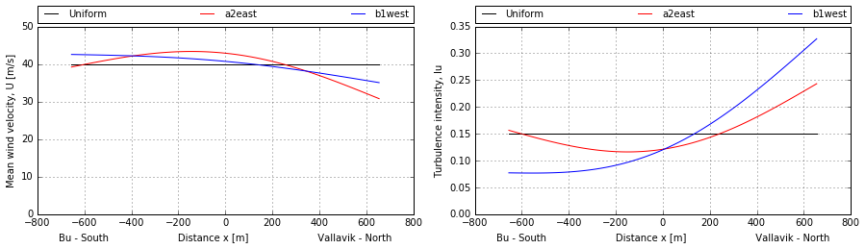

Fig. 5 Extreme non-uniform wind profiles used in buffeting calculations

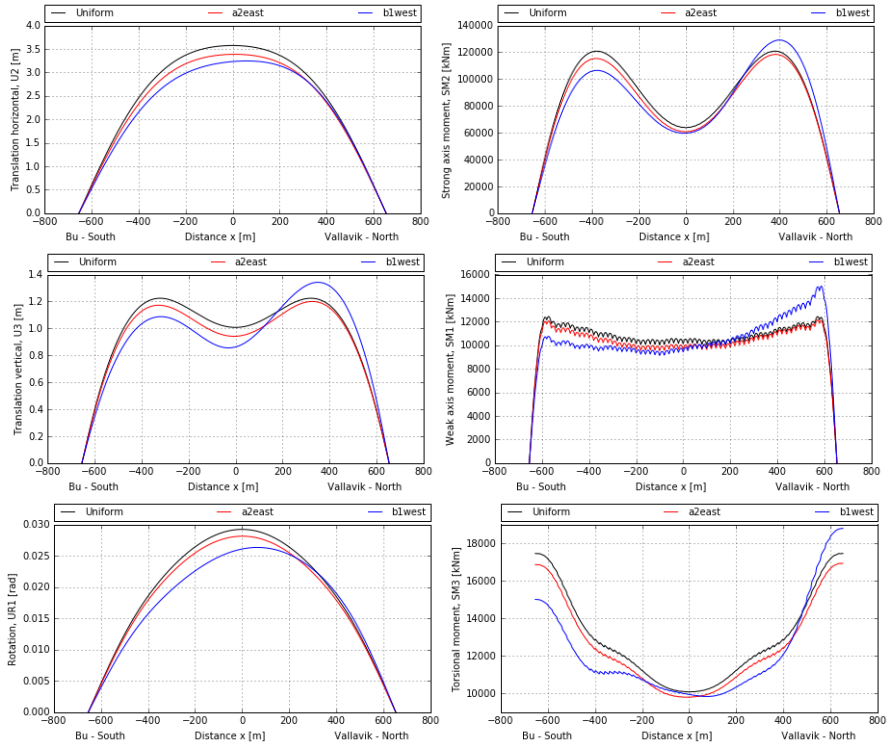

Fig. 6 Along span buffeting response of the Hardanger Bridge subjected to different wind profiles

6 Conclusions

A proposed method for investigating extreme non-uniformity effects for long-span bridges has been presented in this study. Measured full-scale wind profiles from the

complex terrain of the Hardanger Bridge site are used as basis for simulation of extreme, but realistic non-uniform profiles of mean wind velocity and along-wind turbulence intensity and the following conclusions are drawn:

- The measured wind field profiles for westerly winds show a linearly varying trend. The easterly winds display a more typical effect where mean wind velocity is larger in the midspan than towards the bridge ends, and the opposite is the case for the turbulence intensity, due to terrain roughness changes along the span.
- A larger randomness in the correlation between the normalized non-uniformity coefficients was observed for the westerly winds than the easterly winds, indicating a dependence between the observed non-uniformity and the upstream terrain complexity.
- In complex terrain, extreme non-uniformity in the wind field can be expected, to the extent that should not be neglected in design of long-span bridges.
- The inverse nature of the mean wind velocity and the corresponding turbulence intensity will to some extent cancel out the non-uniformity effects on the buffeting response. So, to investigate extreme effects due to non-uniformity, an unfavourable combination of mean wind speed and turbulence intensity should be considered.

Acknowledgements The research presented in this study has been financed by the Norwegian Public Roads Administration (NPRA), the Norwegian Research Council and Norconsult AS. The authors appreciate all these contributions.

References

Arena, A., Lacarbonara, W., Valentine, D. T., and Marzocca, P. (2014). "Aeroelastic behavior of long-span suspension bridges under arbitrary wind profiles." *Journal of Fluids and Structures*, 50, 105–119.

Chen, X., Kareem, A., and Matsumoto, M. (2001). "Multimode coupled flutter and buffeting analysis of long span bridges." *Journal of Wind Engineering and Industrial Aerodynamics*, Elsevier, 89(7–8), 649–664.

Dassault Systèmes, Waltham, M. (n.d.). "ABAQUS."

Davenport, A. G. (1962). "Buffeting of a suspension bridge by storm winds." *Journal of the Structural Division*, 88(3), 233–270.

Fenerci, A., and Øiseth, O. (2017). "Measured buffeting response of a long-span suspension bridge compared with numerical predictions based on design wind spectra." *Journal of Structural Engineering*, 143(9).

Fenerci, A., Øiseth, O., and Rönnquist, A. (2017). "Long-term monitoring of wind field characteristics and dynamic response of a long-span suspension bridge in complex terrain." *Engineering Structures*.

Hu, L., Xu, Y., Zhu, Q., Guo, A., and Kareem, A. (2017). "Tropical Storm – Induced Buffeting Response of Long-Span Bridges : Enhanced Nonstationary Buffeting Force Model." *Journal of Structural Engineering*, 143(6), 4017027.

Jain, A., Jones, N. P., and Scanlan, R. H. (1996a). "Coupled flutter and buffeting analysis." *Journal of Structural Engineering*, 122(7), 716–725.

Jain, A., Jones, N. P., and Scanlan, R. H. (1996b). "Coupled aeroelastic and aerodynamic response analysis of long-span bridges." *Journal of Wind Engineering and Industrial Aerodynamics*, Elsevier, 60, 69–80.

Lystad, T. M., Fenerci, A., and Øiseth, O. (2018). "Evaluation of mast measurements and wind tunnel terrain models to describe spatially variable wind field characteristics for long-span bridge design." *Journal of Wind Engineering and Industrial Aerodynamics*, Submitted.

Scanlan, R. H., and Tomko, J. J. (1971). "Airfoil and bridge deck flutter derivatives." *Journal of the Engineering Mechanics Division*, 97(6), 1717–1737.

Siedziako, B., Øiseth, O., and Rønnquist, A. (2017). "An enhanced forced vibration rig for wind tunnel testing of bridge deck section models in arbitrary motion." *Journal of Wind Engineering and Industrial Aerodynamics*, Elsevier, 164, 152–163.

Zhang, X. (2007). "Influence of some factors on the aerodynamic behavior of long-span suspension bridges." *Journal of Wind Engineering and Industrial Aerodynamics*, Elsevier, 95(3), 149–164.